Advances in Nano Research, *Vol. 13, No.4 (2022) 369-378*
https://doi.org/10.12989/anr.2022.13.4.369

Dynamic analysis of viscoelastic concrete plates containing nanoparticle subjected to low velocity impact load

Jijun Luo*[1], Meng Lv[2], Suxia Hou[3], Mohsen Nasihatgozar[4] and Amir Behshad[5]

[1]*Shaanxi Engineering Research Center of Controllable Neutron Source, Xijing University of School of Electronic Information, Xijing University, Xi'an 710123, Shaanxi, China*
[2]*China Construction Seventh Engineering Division Corp., LTD., Zhengzhou 450000, Henan, China*
[3]*Shaanxi Engineering Research Center of Controllable Neutron Source, Xijing University of School of Electronic Information, Xijing University, Xi'an 710123, Shaanxi, China*
[4]*Department of mechanical engineering, Kashan Branch, Islamic Azad University, Kashan, Iran*
[5]*Faculty of Technology and Mining, Yasouj University, Choram 75761-59836, Iran*

(*Received January 7, 2021, Revised August 30, 2022, Accepted September 14, 2022*)

Abstract. Dynamic study of concrete plates under impact load is presented in this article. The main objective of this work is presenting a mathematical model for the concrete plates under the impact load. The concrete plate is reinforced by carbon nanoparticles which the effective material proprieties are obtained by mixture's rule. Impacts are assumed to occur normally over the top layer of the plate and the interaction between the impactor and the structure is simulated using a new equivalent three-degree-of-freedom (TDOF) spring–mass–damper (SMD) model. The structure is assumed viscoelastic based on Kelvin-Voigt model. Based on the classical plate theory (CPT), energy method and Hamilton's principle, the motion equations are derived. Applying DQM, the dynamic deflection and contact force of the structure are calculated numerically so that the effects of mass, velocity and height of the impactor, volume percent of nanoparticles, structural damping and geometrical parameters of structure are shown on the dynamic deflection and contact force. Results show that considering structural damping leads to lower dynamic deflection and contact force. In addition, increasing the volume percent of nanoparticles yields to decreases in the deflection.

Keywords: concrete plate; CPT; low velocity impact; nanoparticles; numerical method

1. Introduction

One of the most common structural elements that may be exposed to impact is plates. Plates are widely used in building structures and bridges and are usually made of concrete. Impact load is a kind of impulsive dynamic load which is disregarded in the design process of plates like other structural members. The main reason for the lack of sufficient research to explore the effect of impact on plates is the fact that the analyses and design of structures subjected to dynamic impact loading are generally very complicated, and such investigates are more difficult when working with inelastic materials, such as concrete.

The dynamic behavior of axially loaded concrete reinforced square column was studied by Amoli *et al*. (2018) experimentally. The deformation mechanics of the composite sandwich beams with smart composite face sheets was calculated by Arbabi *et al*. (2017). An experimental work for considering the dynamic behaviour of reinforced aggregate concrete beams was presented by Azmi *et al*. (2019). Bakhshande Amnieh *et al*. (2018) studied the dynamic response of reinforced concrete plate under blast. A novel three-dimensional (3D) method to simulate projectile penetration into the reinforced concrete beam was considered by Faramoushjan *et al*. (2021). Numerical studies on the vibration of plate was prepared by Farokhian and Kolahchi (2020). The behavior of different reinforced and unreinforced smart plates was reviewed by Fakhar and Kolahchi (2018) based on experiments by Split Hopkinson Pressure Bar. Golabchi *et al*. (2018) proposed an efficient FE model of pre-stressed concrete plate under missile impact considering the effects of damping, erosion, and pre-stressing values (Ghorbanpour Arani *et al*. 2016). Hajmohammad *et al*. (2017, 2018a, b, c, 2019a, b, 2021) focused on the effects of the support types and the support layouts on the dynamic responses and the failure modes of plates subjected to dynamical loads. Heidarzadeh *et al*. (2018) investigated the influence of various parameters such as the rebar's material, amount and arrangement of GFRP, concrete strength on mechanical behavior of reinforced concrete plates. Jafarian Arani (2016) investigated the combination effect of steel and FRP bars on impact response of concrete plates. Numerical results revealed that using hybrid FRP-steel reinforcing growths energy absorption of plate. Jassas *et al*. (2019) executed both experimental and numerical study for considering the impact behavior of two ways simply supported CFRP strips strengthened RC plates. Jamali *et al*. (2016, 2019) developed a failure analytical model to assess the characteristics of reinforced concrete plates under oblique perforation by a rigid projectile. Javano *et al*. (2019) presented the impact response of CFRP-strengthened RC panels under the impact of non-deformable projectiles.

*Corresponding author, Ph.D.,
E-mail: hsxljj@sina.com

ISSN: 2287-237X (Print), 2287-2388 (Online)

Based on an analytical approach, the free Low velocity impact and transient response of FG piezoelectric cylindrical panels subjected to impulsive loads were presented by Jafari Natanzi (2018). Keshtegar *et al*. (2018, 2020a, b, c) investigated active Low velocity impact control of piezoelectric bonded smart structures using PID algorithm. Kolahdouzan *et al*. (2020) considered the impact force on the CNT-reinforced composite plates integrated with piezoelectric layers using Reddy's higher-order shear deformation theory. Motezaker *et al*. (2017a, b, 2021) carried out the analysis of dynamic responses of CNT reinforced composite plates subjected to impact loading. Naseri Taheri *et al*. (2020) studied experimental study on shear behaviors of partial precast steel reinforced concrete beams. Taherifar *et al*. (2020, 2021) presented structural lightweight concrete containing expanded poly-styrene beads.

None of the above mentioned works have studied the impact response of the concrete plates based on numerical solution. The aims and objectives of this paper are presenting a mathematical model for the concrete plates under impact load, numerical solution based on DQM, assuming the effect of nanoparticles and assuming a comprehensive model for the impact simulation. In the present study, low velocity impact of concrete plate is investigated. The concrete plate is reinforced by carbon nanoparticles which the effective material proprieties are obtained by mixture's rule. Applying CPT, the motion equations are obtained based on Hamilton's principal. Spring – mass models are used extensively for analyzing the dynamics of impact. DQM is applied for obtaining the dynamic deflection and contact force of the system. The effects of mass, velocity and height of impactor, boundary conditions, structural damping and geometrical parameters of structure are shown on the dynamic deflection and contact force of system.

2. Strain relations

The schematic of concrete plate containing nanoparticle with length *a*, width *b* and thickness *h* is shown in Fig. 1 subjected to an impactor with mass of *m*, velocity of V_0 and height of *H*.

Based on CPT, the displacement field can be expressed as (Mosharrafian *et al*. 2016, Zamanian *et al*. 2017, Zamani *et al*. 2017, Zarei *et al*. 2017)

$$U_1(x,y,z,t)=U(x,y,t)-z\frac{\partial W}{\partial x} \tag{1}$$

$$U_2(x,y,z,t)=V(x,y,t)-z\frac{\partial W}{\partial y} \tag{2}$$

$$U_3(x,y,z,t)=W(x,y,t), \tag{3}$$

where (U,V) denote the displacement components in x- and y- directions, respectively. In addition, W are bending and shear transverse deflections, respectively. Based on above relations, the strain-displacement equations may be written as

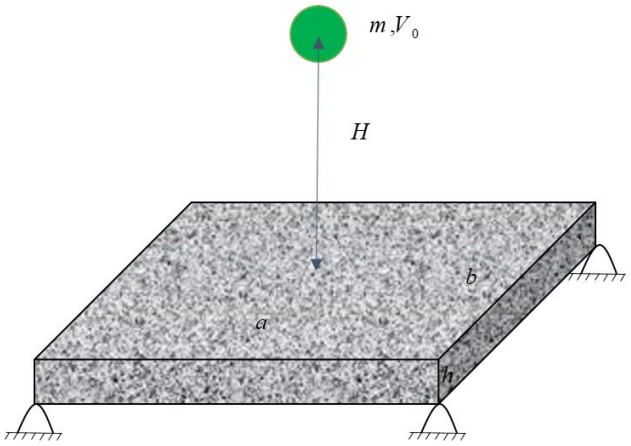

Fig. 1 A schematic of concrete plate subjected to an impactor containing nanoparticle

$$\begin{pmatrix}\varepsilon_{xx}\\ \varepsilon_{yy}\\ \gamma_{xy}\end{pmatrix}=\begin{pmatrix}\varepsilon^0_{xx}\\ \varepsilon^0_{yy}\\ \gamma^0_{xy}\end{pmatrix}+z\begin{pmatrix}k_{xx}\\ k_{yy}\\ k_{xy}\end{pmatrix} \tag{4}$$

$$\begin{pmatrix}\gamma_{yz}\\ \gamma_{xz}\end{pmatrix}=\begin{pmatrix}0\\ 0\end{pmatrix} \tag{5}$$

where ε^0_{ij}, k^b_{ij} and k^s_{ij} are mid plane strains, bending and shear curvatures, respectively which are

$$\begin{pmatrix}\varepsilon^0_{xx}\\ \varepsilon^0_{yy}\\ \gamma^0_{xy}\end{pmatrix}=\begin{pmatrix}\dfrac{\partial U}{\partial x}\\ \dfrac{\partial V}{\partial y}\\ \dfrac{\partial U}{\partial y}+\dfrac{\partial V}{\partial x}\end{pmatrix},\quad \begin{pmatrix}k_{xx}\\ k_{yy}\\ k_{xy}\end{pmatrix}=\begin{pmatrix}-\dfrac{\partial^2 W}{\partial x^2}\\ -\dfrac{\partial^2 W}{\partial y^2}\\ -2\dfrac{\partial^2 W}{\partial x\,\partial y}\end{pmatrix}, \tag{6a}$$

$$\begin{pmatrix}\gamma^s_{yz}\\ \gamma^s_{xz}\end{pmatrix}=\frac{-4}{h^3}\begin{pmatrix}\dfrac{\partial W_s}{\partial y}\\ \dfrac{\partial W_s}{\partial x}\end{pmatrix} \tag{6b}$$

3. Stress-strain relations

Based on Hook's law, the stress-strain relation of the concrete plate can be written as (Kolahchi *et al*. 2020):

$$\begin{bmatrix}\sigma_{xx}\\ \sigma_{yy}\\ \sigma_{zz}\\ \sigma_{zy}\\ \sigma_{xz}\\ \sigma_{zy}\end{bmatrix}=\begin{bmatrix}C_{11}&C_{12}&C_{13}&0&0&0\\ C_{12}&C_{22}&C_{23}&0&0&0\\ C_{13}&C_{23}&C_{33}&0&0&0\\ 0&0&0&C_{44}&0&0\\ 0&0&0&0&C_{55}&0\\ 0&0&0&0&0&C_{66}\end{bmatrix}\begin{bmatrix}\varepsilon_{xx}\\ \varepsilon_{yy}\\ \varepsilon_{zz}\\ \gamma_{zy}\\ \gamma_{xz}\\ \gamma_{xy}\end{bmatrix}, \tag{7a}$$

where σ_{ij}, ε_{ij} and C_{ij} are stress, strain and elastic

constants, respectively. The elastic constants can be obtained by Mixture's rule as:

$$C_{ij} = C_{ij}^{n} V_n + C_{ij}^{m} \left(1 - V_n\right) \tag{7b}$$

where super index "n: is related to nanoparticles and super index "m" is related to matrix. In addition, V_n, is volume percent of nanoparticle.

4. Energy method

The potential energy (U) can be written as

$$U = \frac{1}{2}\int_A \int_{-\frac{h}{2}}^{\frac{h}{2}} \left(\begin{array}{l} \sigma_{xx}\varepsilon_{xx} + \sigma_{yy}\varepsilon_{yy} \\ + \sigma_{xy}\gamma_{xy} + \sigma_{xz}\gamma_{xz} + \sigma_{yz}\gamma_{yz} \end{array} \right) dz\, dA \tag{8}$$

Combining of Eqs. (1)-(3) and (8) yields

$$\begin{aligned} U = \frac{1}{2}\int_A \Bigg(& N_{xx}\frac{\partial U}{\partial x} + N_{xy}\frac{\partial U}{\partial y} + N_{xy}\frac{\partial V}{\partial x} \\ & + N_{yy}\frac{\partial V}{\partial y} - M_{xx}\frac{\partial^2 W}{\partial x^2} - M_{yy}\frac{\partial^2 W}{\partial y^2} - 2M_{xy}\frac{\partial^2 W}{\partial y\, \partial x} \Bigg) \mathrm{dA}, \end{aligned} \tag{9}$$

where the stress resultant-displacement relations can be written as

$$\begin{bmatrix} N_{xx} \\ N_{yy} \\ N_{xy} \end{bmatrix} = \int_{-h}^{h} \begin{bmatrix} \sigma_{xx} \\ \sigma_{yy} \\ \sigma_{xy} \end{bmatrix} dz \tag{10}$$

$$\begin{bmatrix} M_{xx} \\ M_{yy} \\ M_{xy} \end{bmatrix} = \int_{-h}^{h} \begin{bmatrix} \sigma_{xx} \\ \sigma_{yy} \\ \sigma_{xy} \end{bmatrix} z\, dz \tag{11}$$

Substituting stress-strain relation into Eqs. (10) and (11), the stress resultant-displacement relations can be obtained as follow

$$N_{xx} = A_{11}\frac{\partial}{\partial x}U - A_{11z}\frac{\partial^2}{\partial x^2}W + A_{12}\frac{\partial}{\partial y}V - A_{12z}\frac{\partial^2}{\partial y^2}W_s, \tag{12}$$

$$N_{yy} = A_{21}\frac{\partial}{\partial x}U - A_{21z}\frac{\partial^2}{\partial x^2}W + A_{22}\frac{\partial}{\partial y}V - A_{22z}\frac{\partial^2}{\partial y^2}W, \tag{13}$$

$$N_{xy} = A_{44}\frac{\partial}{\partial y}U + A_{44}\frac{\partial}{\partial x}V - 2A_{44z}\frac{\partial^2}{\partial x\, \partial y}W \tag{14}$$

$$M_{xx} = A_{11z}\frac{\partial}{\partial x}U - B_{11}\frac{\partial^2}{\partial x^2}W - A_{12z}\frac{\partial}{\partial y}V - B_{12}\frac{\partial^2}{\partial y^2}W, \tag{15}$$

$$M_{yy} = A_{21z}\frac{\partial}{\partial x}U - B_{21}\frac{\partial^2}{\partial x^2}W + A_{22z}\frac{\partial}{\partial y}V - B_{22}\frac{\partial^2}{\partial y^2}W \tag{16}$$

$$M_{xy} = 2A_{44z}\frac{\partial}{\partial y}U + 2A_{44z}\frac{\partial}{\partial x}V - 2B_{44}\frac{\partial^2}{\partial x\, \partial y}W, \tag{17}$$

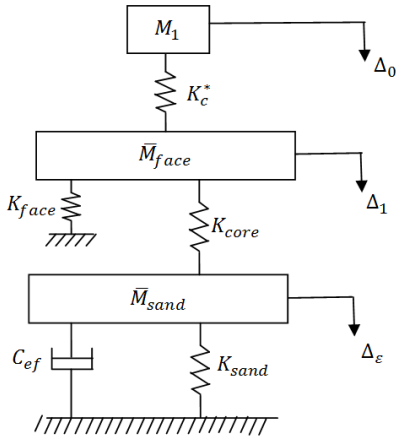

Fig. 2 The equivalent TDOF model of the structure and the impactor system (SMD model)

where

$$\left(A_{11}, A_{12}, A_{22}, A_{44}\right) = \int_{-h}^{h} \left(C_{11}, C_{12}, C_{22}, C_{44}\right) dz, \tag{18}$$

$$\left(A_{11z}, A_{12z}, A_{22z}, A_{44z}\right) = \int_{-h}^{h} \left(C_{11}, C_{12}, C_{22}, C_{44}\right) z\, dz, \tag{19}$$

$$\left(B_{11}, B_{12}, B_{22}, B_{44}\right) = \int_{-h}^{h} \left(C_{11}, C_{12}, C_{22}, C_{44}\right) z^2\, dz, \tag{20}$$

The kinetic energy (K) of system may be written as

$$K = \frac{1}{2}\rho \int_A \int_{-\frac{h}{2}}^{\frac{h}{2}} \left(\left(\frac{\partial u}{\partial t}\right)^2 + \left(\frac{\partial v}{\partial t}\right)^2 + \left(\frac{\partial w}{\partial t}\right)^2 \right) \mathrm{dz\, dA}. \tag{21}$$

5. Low-velocity impact of structure

As shown in Fig. 2, the three-degrees-of-freedom (TDOF) spring–mass–damper (SMD) model is applied to predict the low-velocity impact response of concrete plate (Xu *et al*. 2020).

The motion equations of the three-TDOF system can be written as follows:

$$M_I \ddot{\Delta}_0 + K_C^*(\Delta_0 - \Delta_1) = 0 \tag{22}$$

$$\begin{aligned} & \bar{M}_{face}\ddot{\Delta}_1 + K_{face}\Delta_1 + K_{face}(\Delta_1 - \Delta_2) \\ & + K_C^*(\Delta_1 - \Delta_0) = 0 \end{aligned} \tag{23}$$

$$\bar{M}_{sand}\ddot{\Delta}_2 + K_{sand}\Delta_2 + K_{core}(\Delta_2 - \Delta_1) + C_{ef}\dot{\Delta}_2 = 0 \tag{24}$$

where Δ_0, Δ_1 and Δ_2 are transverse displacements of impactor, impacted top and bottom face sheets, respectively, M_I, $\bar{M}_{face}$ and $\bar{M}_{sand}$ are the mass of impactor, effective mass of impacted face sheet and effective mass of concrete plate, respectively, K_C^*, K_{face}, K_{sand} and K_{core} are respectively, effective stiffness of contact, face sheet, concrete plate and core, C_{ef} is the effective viscous damping coefficient which can be defined as

$$C_{ef} = \eta_{st}\left(K_{stand} / \omega_1\right), \tag{25}$$

where η_{st} and ω_1 are damping coefficient and fundamental natural frequency of structure, respectively. The effective stiffness of impactor can be expressed as

$$K_C^* = \sqrt{\pi}\Gamma\left(\frac{P+1}{2}\right)\frac{2\Gamma\left(\frac{P}{2}+1\right)+\sqrt{\pi}\Gamma\left(\frac{P+1}{2}\right)}{4\Gamma^2\left(\frac{P}{2}+1\right)+\pi\Gamma^2\left(\frac{P+1}{2}\right)}\alpha_{max}^{P-1}K_{c,} \tag{26}$$

where Γ is gamma function, P is Hertzian indentation (usually $P=1.5$), α_{max} is a parameter which can be written as:

$$\alpha_{max} = \left(\frac{\bar{M}_{sand}\cdot M_1}{\bar{M}_{sand}+M_1}\right)^{\frac{1}{(P+1)}}\left(\frac{P+1}{2}\right)^{\frac{1}{(P+1)}}\left(\frac{V_0^2}{K_c}\right)^{\frac{1}{(P+1)}} \tag{27}$$

where V_0 is the impact velocity of impactor and the contact stiffness (K_c) may be estimated as

$$K_c = \left(\frac{4}{3}\right)E_I R_I^{1/2}, \frac{1}{E_I} = \frac{1-\nu_I^2}{E_I} + \frac{1-\nu_P^2}{E_P} \tag{28}$$

where R_I, E_I and υ_I are radius, elastic modulus and poison's ratio of impactor, respectively, E_p and υ_p are elastic modulus and poison's ratio of structure, respectively.

The effective compressive stiffness of elastic flexible core can be given as follows (Chow *et al*. 1992):

$$K_{core} = 8\sqrt{k_F D_f^*} \tag{29}$$

where k_F is the foundation stiffness (elastic region of the core is modeled as a Winkler foundation) and D_f^* is the effective stiffness of the impacted face sheet which can be written as

$$D_f^* = \sqrt{D_{11}D_{22}(\gamma+1)/2} \tag{30}$$

$$\gamma = (D_{12}+2D_{66})/\sqrt{D_{11}D_{22}} \tag{31}$$

$$k_F = \frac{E_c}{\bar{h}_c} \tag{32}$$

where D_{ij} are bending rigidity constants, E_c is the concrete Young's modulus and $\bar{h}_c$ can be expressed as

$$\begin{aligned} &\bar{h}_c = \frac{h_c}{1.38} \quad for \quad h_c \le h_{c\,max} \\ &and \quad \bar{h}_c = 2h_{c\,max} \quad for \quad h_c > h_{c\,max} \end{aligned} \tag{33}$$

$$\bar{h}_c = \left(\frac{27}{64}\right)^2 2h_{c\,max} \quad for \quad h_c > h_{c\,max} \tag{34}$$

$$h_{c\,max} \approx h_f\left(\frac{32}{27}\right)\left(\frac{4Q_f^*}{3E_c}\right)^{1/3} where \quad Q_f^* = \frac{12D_f^*}{h_f^3} \tag{35}$$

where h_f is the thickness of the impacted face sheet. The system of ordinary differential eequation can be solved analytically using the following initial conditions:

$$\Delta_0(t=0)=0,\ \Delta_1(t=0)=0,\ \Delta_2(t=0)=0, \tag{36}$$

$$\dot{\Delta}_0(t=0)=V_0,\ \dot{\Delta}_1(t=0)=0,\ \dot{\Delta}_2(t=0)=0, \tag{37}$$

By applying the equivalent, the eigenvalue equation can be obtained. Therefore,

$$\begin{aligned} &\left(M_I\bar{M}_{face}\bar{M}_{sand}\right)\lambda^{*3} - \begin{bmatrix} K_{gbc}\bar{M}_{face}M_I + K_{gcc}\bar{M}_{sand}M_I \\ +K_C^*\bar{M}_{face}\bar{M}_{sand} \end{bmatrix}\lambda^{*2} \\ &+\begin{bmatrix} M_I\left(K_{gcc}K_{gbc}-K_{core}^2\right) \\ +K_C^*\left(K_{gbc}\bar{M}_{face}+K_{gcc}\bar{M}_{sand}\right)-K_c^{*2}\bar{M}_{sand} \end{bmatrix}\lambda^* \\ &+\left[K_c^{*2}K_{gbc}-K_C^*\left(K_{gcc}K_{gbc}-K_{core}^2\right)\right]=0 \end{aligned} \tag{38}$$

where

$$K_{gcc} = K_{face} + K_{core} + K_C^* \tag{39}$$

$$K_{gbc} = K_{sand}(1+\eta_{st}j) + K_{core} \tag{40}$$

$$j = \sqrt{-1} \tag{41}$$

The above eigenvalue equation has complex coefficients of $\lambda^* = \lambda' + i\lambda''$ where the circular frequency is $\omega = \sqrt{\lambda'}$. Finally, the equivalent contact force can be obtained as

$$\begin{aligned} [F_c^*(t) = K_C^*\big[&c_1\left(\phi_0^1-1\right)\sin(\omega_1 t) + c_2\left(\phi_0^2-1\right)\sin(\omega_2 t) \\ &+ c_3\left(\phi_0^3-1\right)\sin(\omega_3 t)\big] \end{aligned} \tag{42}$$

where

$$\begin{aligned} &\phi_0^i = real\left(\frac{K_C^*}{K_C^* - M_I\lambda^*}\right), \\ &\phi_2^i = real\left(\frac{K_{core}}{K_{gbc}-\bar{M}_{sand}^*\lambda^*}\right) \quad , \ i = 1,2,3 \end{aligned} \tag{43}$$

$$c_1 = \frac{-V_0(\phi_2^2-\phi_2^3)}{\omega_1[(\phi_0^2-\phi_0^1)(\phi_2^1-\phi_2^3)-(\phi_2^2-\phi_2^1)(\phi_0^1-\phi_0^3)]} \tag{44}$$

$$c_2 = \frac{V_0(\phi_2^1-\phi_2^3)}{\omega_2[(\phi_0^2-\phi_0^1)(\phi_2^1-\phi_2^3)-(\phi_2^2-\phi_2^1)(\phi_0^1-\phi_0^3)]} \tag{45}$$

$$c_3 = \frac{-V_0(\phi_2^1-\phi_2^2)}{\omega_2[(\phi_0^2-\phi_0^1)(\phi_2^1-\phi_2^3)-(\phi_2^2-\phi_2^1)(\phi_0^1-\phi_0^3)]} \tag{46}$$

The governing equations can be derived by Hamilton's principal as follows

$$\int_0^t(\delta U - \delta K - \delta W_e)dt = 0. \tag{47}$$

where W_e is the external force by impact load. Substituting above relations into Eq. (47) yields the following governing equations

$$\frac{\partial}{\partial x}N_{xx} + \frac{\partial}{\partial y}N_{xy} - I_0\frac{\partial^2 U}{\partial t^2} + I_1\frac{\partial^3 W}{\partial x\,\partial t^2} = 0, \tag{48}$$

$$\frac{\partial}{\partial x}N_{xy} + \frac{\partial}{\partial y}N_{yy} - I_0\frac{\partial^2 V}{\partial t^2} + I_1\frac{\partial^3 W}{\partial y\,\partial t^2} = 0, \tag{49}$$

$$\begin{aligned} &\frac{\partial^2}{\partial x^2}M_{xx} + 2\frac{\partial^2}{\partial x\,\partial y}M_{xy} + \frac{\partial^2}{\partial y^2}M_{yy} - I_0\left(\frac{\partial^2 W}{\partial t^2}\right) \\ &-I_1\left(\frac{\partial^3 U}{\partial x\,\partial t^2} + \frac{\partial^3 V}{\partial y\,\partial t^2}\right) + I_2\left(\frac{\partial^4 W}{\partial x^2\partial t^2}\right) = F_c^*(t), \end{aligned} \tag{50}$$

where

$$\left(I_0, I_1, I_2\right)=\int_{-h}^{h}\rho\left(1, z, z^2\right)\mathrm{d}z. \tag{51}$$

Substituting Eqs. (12) to (17) into Eqs. (48) to (50), the governing equations can be written as follow

$$\begin{aligned}&\frac{\partial}{\partial x}\left(A_{11}\frac{\partial}{\partial x}U-A_{11z}\frac{\partial^2}{\partial x^2}W+A_{12}\frac{\partial}{\partial y}V-A_{12z}\frac{\partial^2}{\partial y^2}W\right)\\&+\frac{\partial}{\partial y}\left(A_{44}\frac{\partial}{\partial y}U+A_{44}\frac{\partial}{\partial x}V-2A_{44z}\frac{\partial^2}{\partial x\,\partial y}W\right)\\&=\left[I_0\frac{\partial^2 U}{\partial t^2}-I_1\frac{\partial^3 W}{\partial x\,\partial t^2}\right],\end{aligned} \tag{52}$$

$$\begin{aligned}&\frac{\partial}{\partial x}\left(A_{44}\frac{\partial}{\partial y}U+A_{44}\frac{\partial}{\partial x}V-2A_{44z}\frac{\partial^2}{\partial x\,\partial y}W\right)\\&+\frac{\partial}{\partial y}\left(A_{21}\frac{\partial}{\partial x}U-A_{21z}\frac{\partial^2}{\partial x^2}W+A_{22}\frac{\partial}{\partial y}V-A_{22z}\frac{\partial^2}{\partial y^2}W\right)\\&=\left[I_0\frac{\partial^2 V}{\partial t^2}-I_1\frac{\partial^3 W}{\partial y\,\partial t^2}\right],\end{aligned} \tag{52}$$

$$\begin{aligned}&\frac{\partial^2}{\partial x^2}\left(A_{11z}\frac{\partial}{\partial x}U-B_{11}\frac{\partial^2}{\partial x^2}W+A_{12z}\frac{\partial}{\partial y}V-B_{12}\frac{\partial^2}{\partial y^2}W\right)\\&+2\frac{\partial^2}{\partial x\,\partial y}\left(2A_{44z}\frac{\partial}{\partial y}U+2A_{44z}\frac{\partial}{\partial x}V-2B_{44}\frac{\partial^2}{\partial x\,\partial y}W\right)\\&+\frac{\partial^2}{\partial y^2}\left(A_{21z}\frac{\partial}{\partial x}U-B_{21}\frac{\partial^2}{\partial x^2}W+A_{22z}\frac{\partial}{\partial y}V-B_{22}\frac{\partial^2}{\partial y^2}W\right)\\&=I_0\left(\frac{\partial^3 W_b}{\partial t^2}\right)+I_1\left(\frac{\partial^3 U}{\partial x\,\partial t^2}+\frac{\partial^3 V}{\partial y\,\partial t^2}\right)\\&-I_2\left(\frac{\partial^4 W}{\partial x^2\partial t^2}+\frac{\partial^4 W}{\partial y^2\partial t^2}\right)\Bigg]+F_c^*(\mathrm{t}),\end{aligned} \tag{54}$$

6. Numerical solution

The DQM approximates the partial derivative of a function *F*, with respect to two spatial variables (*x* and *y*) at a given discrete point (x_i, y_i), as a weighted linear sum of the function values at all discrete points chosen in the solution domain ($0 < x < L$, $0 < y < b$) with $Nx \times N_y$ grid points along *x* and *y* axes, respectively. Then, the nth-order partial derivative of $F(x, y)$ with respect to *x*, the mth-order partial derivative of $F(x, y)$ with respect to *y* and the (n + m)th-order partial derivative of $F(x, y)$with respect to both *x* and *y* is expressed discretely at the point (x_i, y_i) as (Al-Furjan *et al*. 2022a, b, c, d, e, f, 2021a, b, c, 2020, Kolahchi *et al*. 2016, 2017a, b, 2018, 2020a, b, 2021, 2022)

$$\frac{d^n F(x_i, y_j)}{dx^n}=\sum_{k=1}^{N_x}A_{ik}^{(n)}F(x_k, y_j) \tag{26}$$

$$\frac{d^m F(x_i, y_j)}{dy^m}=\sum_{l=1}^{N_y}B_{jl}^{(m)}F(x_i, y_l) \tag{27}$$

$$\frac{d^{n+m}F(x_i, y_j)}{dx^n dy^m}=\sum_{k=1}^{N_x}\sum_{l=1}^{N_y}A_{ik}^{(n)}B_{jl}^{(m)}F(x_k, y_l), \tag{28}$$

where $A_{ik}^{(n)}$ and $B_{jl}^{(m)}$ are the weighting coefficients which may be defined as

$$A_{ij}^{(1)}=\begin{cases}\dfrac{M(x_i)}{(x_i-x_j)M(x_j)} & for\quad i\neq j,\quad i,j=1,2,...,N_x\\ -\sum\limits_{\substack{j=1\\ i\neq j}}^{N_x}A_{ij}^{(1)} & for\quad i=j,\quad i,j=1,2,...,N_x\end{cases} \tag{58}$$

$$B_{ij}^{(1)}=\begin{cases}\dfrac{P(y_i)}{(y_i-y_j)P(y_j)} & for\quad i\neq j,\quad i,j=1,2,...,N_y,\\ -\sum\limits_{\substack{j=1\\ i\neq j}}^{N_y}B_{ij}^{(1)} & for\quad i=j,\quad i,j=1,2,...,N_y\end{cases} \tag{59}$$

where M and P are Lagrangian operators which are defined as

$$M(x_i)=\prod_{\substack{j=1\\ j\neq i}}^{N_x}(x_i-x_j) \tag{60}$$

$$P(y_i)=\prod_{\substack{j=1\\ j\neq i}}^{N_y}(y_i-y_j) \tag{61}$$

The weighting coefficients for the second, third and fourth derivatives are determined via matrix multiplication,

$$A_{ij}^{(n)}=n\left(A_{ii}^{(n-1)}A_{ij}^{(1)}-\frac{A_{ij}^{(n-1)}}{(x_i-x_j)}\right) \tag{62}$$

$$B_{ij}^{(m)}=m\left(B_{ii}^{(m-1)}B_{ij}^{(1)}-\frac{B_{ij}^{(m-1)}}{(y_i-y_j)}\right) \tag{63}$$

Using the following rule, the distribution of grid points in domain is calculated as

$$x_i=\frac{L}{2}\left[1-\cos\left(\frac{i-1}{N_x-1}\right)\pi\right]\qquad i=1,...,N_x \tag{64}$$

$$y_i=\frac{b}{2}\left[1-\cos\left(\frac{i-1}{N_y-1}\right)\pi\right]\quad i=1,...,N_y \tag{65}$$

Using DQM, the motion equations for low-velocity impact of structure can be expressed in matrix form as

$$[M]\{\ddot{\chi}\}+[C_e]\{\dot{\chi}\}+[K]\{\chi\}=\{Q\} \tag{66}$$

where $[M]$, $[k]$ and $[C_e]$ are the mass, stiffness and damp matrixes, respectively, $\{\chi\}$ is the dynamic vector, Q is the dynamic load vector. Defining the second and first time derivatives using Teoplitz matrices as follows

$$\begin{cases}a_{11}=0,\\ a_{i,1}=(-1)^{i-1}\cot\left(\frac{\pi(i-1)}{n}\right),\\ a_{1,j}=(-1)^{n-j+1}\cot\left(\frac{\pi(n-j+1)}{n}\right),\\ \mathrm{a}_{i+1,j+1}=a_{ij},\end{cases}\quad i,j=2,3,4,...,n,\ \tilde{D}_t^1=2\pi\left[a_{ij}\right], \tag{67}$$

$$\begin{cases} b_{11} = -\dfrac{n^2}{12} - \dfrac{1}{6}, \\ b_{i,1} = \dfrac{(-1)^{i-1}}{2\sin^2\left(\frac{\pi(i-1)}{n}\right)}, \\ b_{1,j} = \dfrac{(-1)^{n-j+1}}{2\sin^2\left(\frac{\pi(n-j+1)}{n}\right)}, \\ b_{i+1,j+1} = b_{ij}, \end{cases} \quad i, j = 2,3,4,...,n,\ \tilde{D}_t^2 = (2\pi)^2 \left[b_{ij}\right]. \quad (68)$$

Eq. (77) can be written as

$$\left([D_t^2 \otimes M] + [D_t^1 \otimes C_e] + [I_t \otimes K]\right)\chi = [Q], \quad (69)$$

where $\otimes$ notes the Kronecker product and I_t is unit matrix. Finally, solving above equation yields to deflection and contact force of structure which are discussed in next section.

7. Numerical Results and discussion

In order to show the effect of different parameters on the dynamic deflection and contact force of the structure, the concrete plate with Young's modulus of $E_c = 20\,GPa$ and Poisson's ratio of $\nu_c = 0.2$ is considered. The plate is reinforced by carbon nanoparticles by Young's modulus of $E_n = 1\,TPa$ and Poisson's ratio of 0.3.

At the first, we want to discuss about the standard deviation of the results. For example, the data of Figs. 3 and 4 is assumed. For computing the standard deviation, we should calculate:

1-Average of the deflection and contact force

2- The square of the difference of each data value with the mean

3- The variance of the data, which is the mean square of the difference between the data and its mean

4- The root of the variance as the standard deviation of the data

The standard deviation for the deflection and contact force are 0.5517 and 0.4920, respectively which show a good and uniform distribution of data.

The effect of velocity and mass of impactor on the histories of contact force and deflection is demonstrated in Figs. 3 and 4, respectively. As can be seen the contact force and the central deflection of the concrete plate increase with increasing impact velocity of impactor while the contact duration decreases as the impact velocity of impactor increases. The reason is that the higher impact velocity of impactor which accompanies a higher impact energy, requires a larger deflection and accompanying contact force to dissipate it.

The impactor height effect on the histories of contact force and deflection is demonstrated in Figs. 5 and 6, respectively. As can be seen the contact force and the central deflection of the concrete plate increase with increasing impact velocity of impactor while the contact duration decreases as the impact velocity of impactor increases. The reason is that the higher impact velocity of impactor which accompanies a higher impact energy, requires a larger deflection and accompanying contact force to dissipate it.

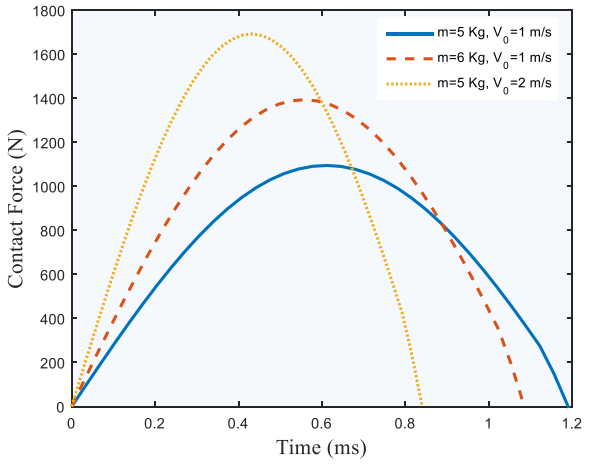

Fig. 3 The impact velocity and mass effect on the history of contact force

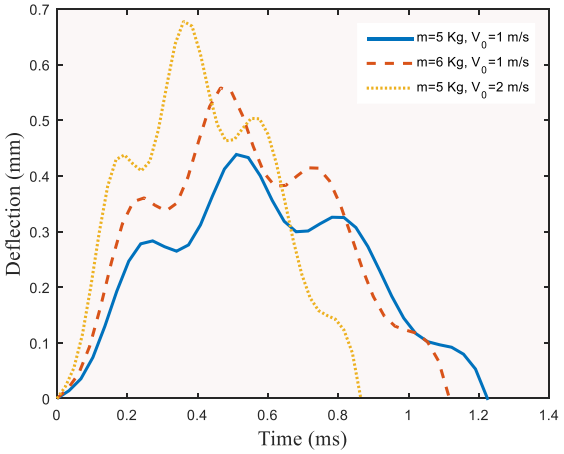

Fig. 4 The impact velocity and mass effect on the history of dynamic deflection

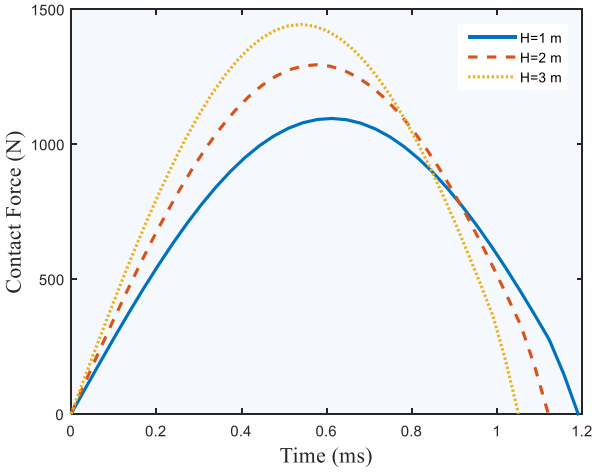

Fig. 5 The impactor height effect on the history of contact force

Figs. 7 and 8 show the effects of nanoparticle volume percent on the contact force and deflection histories of

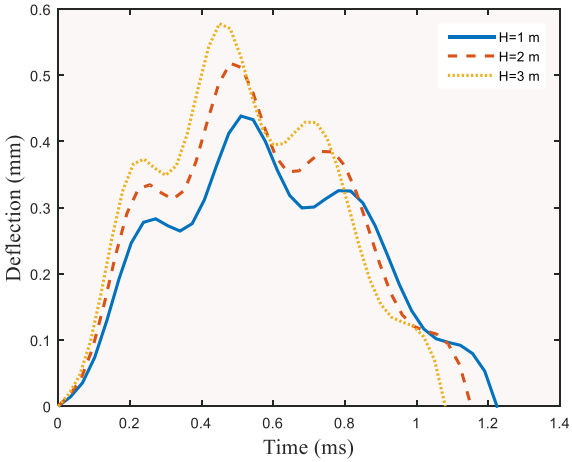

Fig. 6 The impactor height effect on the history of dynamic deflection

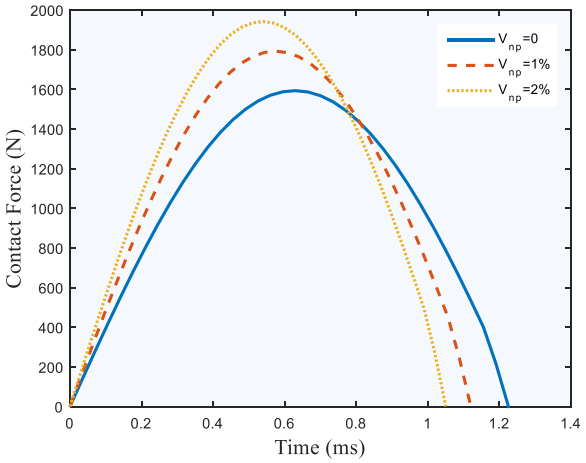

Fig. 7 The nanoparticle volume percent effect on the history of contact force

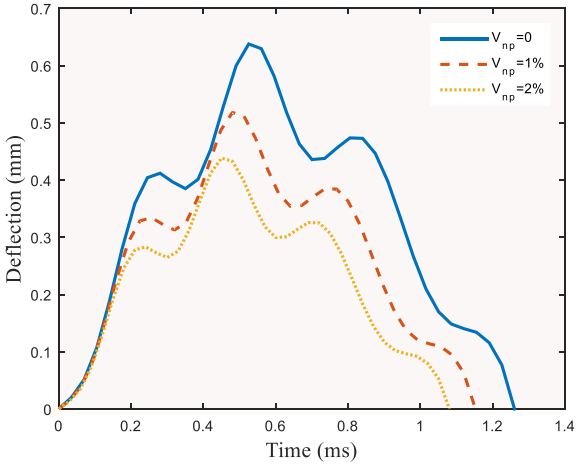

Fig. 8 The nanoparticle volume percent effect on the history of dynamic deflection

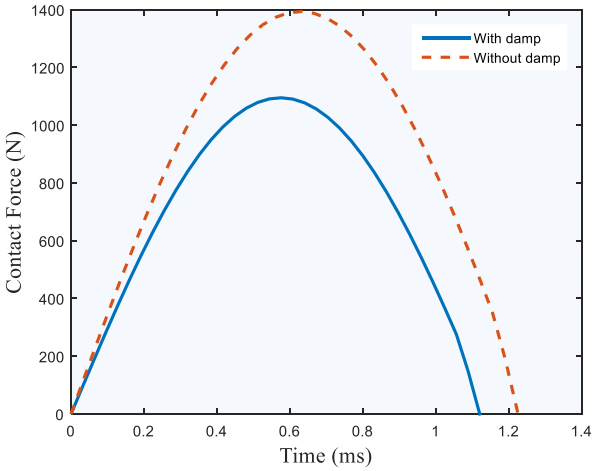

Fig. 9 The structural damping effect on the history of contact force

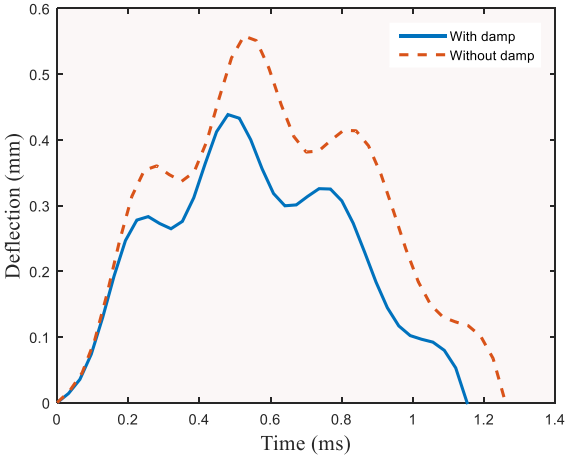

Fig. 10 The structural damping effect on the history of dynamic deflection

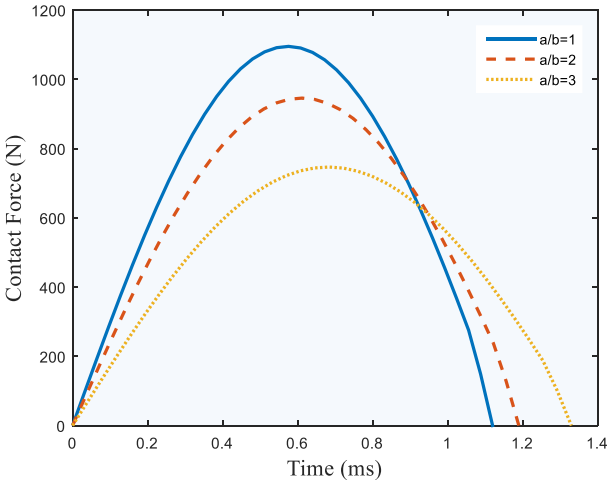

Fig. 11 The length to width ratio of plate effect on the history of contact force

structure, respectively. These figures show that with increasing the nanoparticle volume percent, the maximum contact force decreases slightly. It is since with enhancing the nanoparticle volume percent, the stiffness of the structure is increased. In order to quantitative study, for the concrete plate without nanoparticles, the maximum deflection and contact force are 0.651 mm and 1580 N while these values are 0.43 mm and 1910 N, respectively

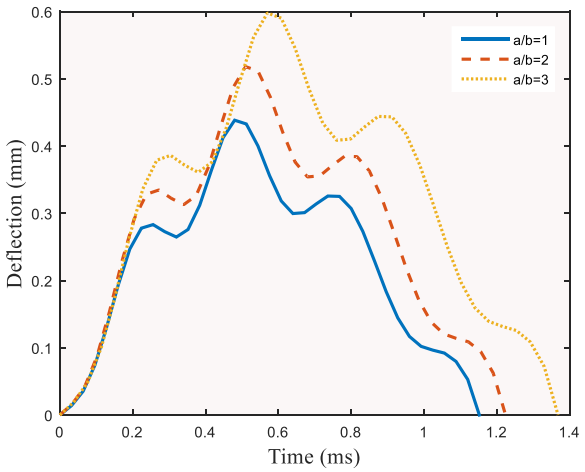

Fig. 12 The length to width ratio of plate effect on the history of dynamic deflection

for volume percent of nanoparticles equal to 2%. In other words, with increasing the the volume percent of nanoparticle, the maximum deflection and contact force are deceased 34% and increased 21%, respectively.

Figs. 9 and 10 depict, respectively contact force and central deflection histories of structure for cases including without structural damping and with structural damping. As can be seen from these figures, considering structural damping decreases the contact force and deflection of the structure.

The effect of the length to width ratio of plate on the contact force and deflection histories is demonstrated in Figs. 11 and 12, respectively. The figure shows that the contact force and the central deflection of the structure increases and the contact time decreases with decreasing length to width ratio of plate. This behavior is due to the decrease of the stiffness with increasing length to width ratio of plate.

8. Conclusions

In this article, low velocity impact response of the concrete plates was presented applying a new equivalent TDOF spring–mass–damper model. The concrete plate is reinforced by carbon nanoparticles which the effective material proprieties are obtained by mixture's rule. Based on CPT, the motion equations were derived using energy method and Hamilton's principle. Exact solution is applied for obtaining the dynamic deflection and contact force of system so that the effects of the of mass, velocity and height of impactor, volume percent of nanoparticles, structural damping and geometrical parameters of structure are shown on the dynamic deflection and contact force of system were considered. Results indicated considering structural damping decreases the contact force and deflection of the structure. In addition, the contact force and the central deflection of the structure increases and the contact time decreases with decreasing length to width ratio of plate. With increasing the the volume percent of nanoparticle, the maximum deflection and contact force were deceased 34% and increased 21%, respectively. Furthermore, the contact force and the central deflection of the structure increase with increasing impact velocity of impactor while the contact duration decreases as the impact velocity of impactor increases.

In this paper, low velocity impact load is assumed with relatively high masses and low impact velocities. In the future works, the high velocity impact of this structure can be novel topic for researchers. High velocity impact loads from scenarios like particle impact, involving comparably small masses and high. It is also noted that for high velocity impact, the stress relations, the elasto-plastic formulation should assumed (Žmindák *et al*. 2016) and for the impact force we should use from a new relations (Alonso and Solis, 2021).

Funding

The authors extend their sincere thanks to the National Nature Science Fund of China Grants Agreement Number 51309228 for the financial support for this work. The author also thanks the Postdoctoral Science Foundation of China for financial supporting this work (No.2013M542459), and Shaanxi Technology Committee Natural Science Basic Research Project for financial supporting this work (No. 2016JM6026).

References

Al-Furjan, M.S.H., Xu, M.X., Farrokhian, A., Jafari, G.S., Shen, X. and Kolahchi, R. (2022a), "On wave propagation in piezoelectric-auxetic honeycomb-2D-FGM micro-sandwich beams based on modified couple stress and refined zigzag theories", *Wave Random Complex. Med*., 1-25. https://doi.org/10.1080/17455030.2022.2030499.

Al-Furjan, M.S.H., Yang, Y., Farrokhian, G.S., Shen, X., Kolahchi, R. and Rajak, D.K. (2022b), "Dynamic instability of nano-composite piezoelectric-leptadenia pyrotechnica rheological elastomer-porous functionally graded materials micro viscoelastic beams at various strain gradient higher-order theories", *Polym. Compos*., **43**, 282-298. https://doi.org/10.1002/pc.26373.

Al-Furjan, M.S.H., Yin, C., Shen, X., Kolahchi, R., Zarei, M.S. and Hajmohammad, M.H. (2022c), "Energy absorption and vibration of smart auxetic FG porous curved conical panels resting on the frictional viscoelastic torsional substrate", *Mech. Syst. Signal Pr*., **178**, 109269. https://doi.org/10.1016/j.ymssp.2022.109269.

Al-Furjan, M.S.H., Shan, L., Shen, X., Zarei, M.S., Hajmohammad, M.H. and Kolahchi, R. (2022d), "A review on fabrication techniques and tensile properties of glass, carbon, and kevlar fiber reinforced polymer composites", *J. Mat. Res. Tech.*, **19**, 2930-2959. https://doi.org/10.1016/j.jmrt.2022.06.008.

Al-Furjan, M.S.H., Shan, L., Shen, X., Kolahchi, R. and Rajak, D.K. (2022e), "Combination of FEM-DQM for nonlinear mechanics of porous GPL-reinforced sandwich nanoplates based on various theories", *Thin-Wall. Struct*., **178**, 109495. https://doi.org/10.1016/j.tws.2022.109495.

Al-Furjan, M.S.H., Kong, X.S., Shan, L., Soleimani Jafari, G., Farrokhian, A., Kolahchi, R. and Rajak, D.K. (2022f), "Influence of LPRE on the size-dependent phase velocity of

sandwich beam including FG porous and smart nanocomposite layers", *Polym. Compos.* https://doi.org/10.1002/pc.26820.

Al-Furjan, M.S.H., Farrokhian, A., Mahmoud, S.R., Kolahchi, R. (2021a), "Dynamic deflection and contact force histories of graphene platelets reinforced conical shell integrated with magnetostrictive layers subjected to low-velocity impact", *Thin Wall. Struct.* **163**, 107706. https://doi.org/10.1016/j.tws.2021.107706.

Al-Furjan, M.S.H., Hajmohammad, M.H., Shen, X., Rajak, D.K. and Kolahchi, R. (2021b), "Evaluation of tensile strength and elastic modulus of 7075-T6 aluminum alloy by adding SiC reinforcing particles using vortex casting method", *J. Alloys. Compd.*, **886**, 161261. https://doi.org/10.1016/j.jallcom.2021.161261.

Al-Furjan, M., Farrokhian, A., Keshtegar, B., Kolahchi, R. and Trung, N.T. (2021c), "Dynamic stability control of viscoelastic nanocomposite piezoelectric sandwich beams resting on Kerr foundation based on exponential piezoelasticity theory", *Eur. J. Mech. A Solids*, **86**, 104169. https://doi.org/10.1016/j.euromechsol.2020.104169.

Al-Furjan, M., Farrokhian, A., Keshtegar, B., Kolahchi, R. and Trung, N.T. (2020), "Higher order nonlocal viscoelastic strain gradient theory for dynamic buckling analysis of carbon nanocones", *Aerosp. Sci. Technol.*, **107**, 106259. https://doi.org/10.1016/j.ast.2020.106259.

Alonso, L. and Solis, A. (2021), "High-velocity impact on composite sandwich structures: A theoretical model", *Int. J. Mech. Sci.*, **201**, 106459. https://doi.org/10.1016/j.ijmecsci.2021.106459.

Amoli, A., Kolahchi, R. and Rabani Bidgoli, M. (2018), "Seismic analysis of AL2O3 nanoparticles-reinforced concrete plates based on sinusoidal shear deformation theory", *Earthq. Struct.* **15**(3), 285-294. https://doi.org/10.12989/eas.2018.15.3.285.

Arbabi, A., Kolahchi, R. and Rabani Bidgoli, M. (2017), "Concrete columns reinforced with Zinc Oxide nanoparticles subjected to electric field: buckling analysis", *Wind Struct.*, **24**(5), 431-446. https://doi.org/10.12989/was.2017.24.5.431.

Azmi, M., Kolahchi, R. and Rabani Bidgoli, M. (2019), "Dynamic analysis of concrete column reinforced with Sio2 nanoparticles subjected to blast load", *Adv. Concr. Constr.*, **7**(1), 51-63. https://doi.org/10.12989/acc.2019.7.1.051.

Bakhshande Amnieh. H., Zamzam, M.S. and Kolahchi, R. (2018), "Dynamic analysis of non-homogeneous concrete blocks mixed by SiO_2 nanoparticles subjected to blast load experimentally and theoretically", *Constr. Build. Mater.*, **174**, 633-644. https://doi.org/10.1016/j.conbuildmat.2018.04.140.

Chow, S.T., Liew, K.M. and Lam, K.Y. (1992), "Transverse Low velocity impact of symmetrically laminated rectangular composite plates", *Compos. Struct.*, **20**, 213-218. https://doi.org/10.1016/j.proeng.2013.09.187.

Faramoushjan, S.G., Jalalifar, H. and Kolahchi, R. (2021), "Mathematical modelling and numerical study for buckling study in concrete beams containing carbon nanotubes", *Adv. Concr. Constr.*, **11**(6), 521-529. https://doi.org/10.12989/acc.2021.11.6.521.

Farokhian, A. and Kolahchi, R. (2020), "Frequency and instability responses in nanocomposite plate assuming different distribution of CNTs", *Struct. Eng. Mech.*, **73**(5), 555-563. https://doi.org/10.12989/sem.2020.73.5.555.

Fakhar, A. and Kolahchi, R. (2018), "Dynamic buckling of magnetorheological fluid integrated by visco-piezo-GPL reinforced plates", *Int. J. Mech. Sci.*, **144**, 788-799. https://doi.org/10.1016/j.ijmecsci.2018.06.036.

Golabchi, H., Kolahchi, R. and Rabani Bidgoli, M. (2018), "Vibration and instability analysis of pipes reinforced by SiO2 nanoparticles considering agglomeration effects", *Comput. Concrete*, **21**, 431-440. https://doi.org/10.12989/cac.2018.21.4.431.

Ghorbanpour Arani, A., Jamali, M., Ghorbanpour-Arani, A.H., Kolahchi, R. and Mosayyebi, M. (2016), "Electro-magneto wave propagation analysis of viscoelastic sandwich nanoplates considering surface effects", *Proc. Inst. Mech. Eng. Part C*, **231**, 1989-1996.https://doi.org/10.1177/0954406215627830.

Hajmohammad, M.H., Sharif Zarei, M., Nouri, A. and Kolahchi, R. (2017), "Dynamic buckling of sensor/functionally graded-carbon nanotube-reinforced laminated plates/actuator based on sinusoidal-visco-piezoelasticity theories", *J. Sandw. Struct. Mater.*, 1099636217720373. https://doi.org/10.1177/1099636217720373.

Hajmohammad, M.H., Azizkhani, M.B. and Kolahchi, R. (2018a), "Multiphase nanocomposite viscoelastic laminated conical shells subjected to magneto-hygrothermal loads: Dynamic buckling analysis", *Int. J. Mech. Sci.*, **137**, 205-213. https://doi.org/10.1016/j.ijmecsci.2018.01.026.

Hajmohammad, M.H., Zarei, M.S., Farrokhian, A. and Kolahchi, R. (2018b), "A layerwise theory for buckling analysis of truncated conical shells reinforced by CNTs and carbon fibers integrated with piezoelectric layers in hygrothermal environment", *Adv. Nano Res.*, **6**(4), 299-321. https://doi.org/10.12989/anr.2018.6.4.299.

Hajmohammad, M.H., Maleki, M. and Kolahchi, R. (2018c), "Seismic response of underwater concrete pipes conveying fluid covered with nano-fiber reinforced polymer layer", *Soil Dyn. Earthq. Eng.*, **110**, 18-27. https://doi.org/10.1016/j.soildyn.2018.04.002.

Hajmohammad, M.H., Nouri, A.H., Zarei, M.S. and Kolahchi, R. (2019a), "A new numerical approach and visco-refined zigzag theory for blast analysis of auxetic honeycomb plates integrated by multiphase nanocomposite facesheets in hygrothermal", *Eng. Comput.*, **35**(4), 1141-1157. https://doi.org/10.1007/s00366-018-0655-x.

Hajmohammad, M.H., Zarei, M.S., Kolahchi, R. and Karami, H. (2019b), "Visco-piezoelasticity-zigzag theories for blast response of porous beams covered by graphene platelet-reinforced piezoelectric layers", *J. Sandw. Struct. Mat.*, 1099636219839175. https://doi.org/10.1177/1099636219839175.

Hajmohammad, M.H., Farrokhian, A. and Kolahchi, R. (2021), "Dynamic analysis in beam element of wave-piercing Catamarans undergoing slamming load based on mathematical modelling", *Ocean Eng.*, **234**, 109269. https://doi.org/10.1016/j.oceaneng.2021.109269.

Heidarzadeh, A., Kolahchi, R. and Rabani Bidgoli, M. (2018), "Concrete pipes reinforced with AL2O3 nanoparticles considering agglomeration: Magneto-thermo-mechanical stress analysis", *Int. J. Civ. Eng.*, **16**(3), 315-322. https://doi.org/10.1007/s40999-016-0130-2.

Jafarian Arani, A. and Kolahchi, R. (2016), "Buckling analysis of embedded laminated porous concrete beams armed with carbon nanotubes", *Comput. Concr.*, **17**, 567-578.

Jassas, M.R., Rabani Bidgoli, M. and Kolahchi, R. (2019), "Forced vibration analysis of concrete plates reinforced by agglomerated SiO_2 nanoparticles based on numerical methods", *Constr. Build. Mater.*, **211**, 796-806. https://doi.org/10.1016/j.conbuildmat.2019.03.263.

Jamali, M., Shojaee, T., Kolahch,i R. and Mohammadi, B. (2016), "Buckling analysis of nanocomposite cut out plate using domain decomposition method and orthogonal polynomials", *Steel Compos. Struct.*, **22**(3), 691-712. https://doi.org/10.12989/scs.2016.22.3.691.

Jamali, M., Shojaee, T., Mohammadi, B. and Kolahchi, R. (2019), "Cut out effect on nonlinear post-buckling behavior of FG-CNTRC micro plate subjected to magnetic field via FSDT", *Adv. Nano Res.*, **7**(6), 405-417.

https://doi.org/10.12989/anr.2019.7.6.405.
Javani, R., Rabani Bidgoli, M. and Kolahchi, R. (2019), "Buckling analysis of plates reinforced by Graphene platelet based on Halpin-Tsai and Reddy theories", *Steel Compos. Struct.*, **31**(4), 419-426. https://doi.org/10.12989/scs.2019.31.4.419.
Jafari Natanzi, A., Soleimani Jafari, G. and Kolahchi, R. (2018), "Vibration and instability of nanocomposite pipes conveying fluid mixed by nanoparticles resting on viscoelastic foundation", *Comput. Concrete*, **21**(5), 569-582. https://doi.org/10.12989/cac.2018.21.5.569.
Keshtegar, B. and Kolahchi, R. (2018), "Reliability analysis-based conjugate map of beams reinforced by ZnO nanoparticles using sinusoidal shear deformation theory", *Steel Compos. Struct.*, **28**(2), 195-20. https://doi.org/10.12989/scs.2018.28.2.195.
Keshtegar, B., Motezaker, M., Kolahchi, R. and Trung, N.T. (2020a), "Wave propagation and vibration responses in porous smart nanocomposite sandwich beam resting on Kerr foundation considering structural damping", *Thin Wall. Struct.* **154**, 106820. https://doi.org/10.1016/j.tws.2020.106820.
Keshtegar, B., Farrokhian, A., Kolahchi, R. and Trung, N.T. (2020b), "Dynamic stability response of truncated nano-composite conical shell with magnetostrictive face sheets utilizing higher order theory of sandwich panels", *Eur. J. Mech. A Solids*, **82**, 104010. https://doi.org/10.1016/j.euromechsol.2020.104010.
Keshtegar, B., Tabatabaei, J., Kolahchi, R. and Trung, N.T. (2020c), "Dynamic stress response in the nanocomposite concrete pipes with internal fluid under the ground motion load", *Adv. Concr. Constr.*, **9**(3), 327-335. https://doi.org/10.12989/acc.2020.9.3.327.
Kolahchi, R., Safari, M. and Esmailpour, M. (2016), "Dynamic stability analysis of temperature-dependent functionally graded CNT-reinforced visco-plates resting on orthotropic elastomeric medium", *Compos. Struct.*, **150**, 255-265. https://doi.org/10.1016/j.compstruct.2016.05.023.
Kolahchi, R. (2017a), "A comparative study on the bending, vibration and buckling of viscoelastic sandwich nano-plates based on different nonlocal theories using DC, HDQ and DQ methods", *Aerosp. Sci. Technol.*, **66**, 235-248. https://doi.org/10.1016/j.ast.2017.03.016.
Kolahchi, R., Zarei, M.S., Hajmohammad, M.H. and Nouri, A.H. (2017b), "Wave propagation of embedded viscoelastic FG-CNT-reinforced sandwich plates integrated with sensor and actuator based on refined zigzag theory", *Int. J. Mech. Sci.* **130** 534-545. https://doi.org/10.1016/j.ijmecsci.2017.06.039.
Kolahchi, R., Hosseini, H., Fakhar, M.H., Taherifar, R. and Mahmoudi, M. (2018), "A numerical method for magneto-hygro-thermal postbuckling analysis of defective quadrilateral graphene sheets using higher order nonlocal strain gradient theory with different movable boundary conditions", *Comput. Math. Appl.*, **78**(6), 2018-2034. https://doi.org/10.1016/j.camwa.2019.03.042.
Kolahchi, R., Zhu, S.P., Keshtegar, B. and Trung, N.T. (2020a). "Dynamic buckling optimization of laminated aircraft conical shells with hybrid nanocomposite martial", *Aerosp. Sci. Technol.*, **98**, 105656, https://doi.org/10.1016/j.ast.2019.105656.
Kolahchi, R., Arbabi, A. and Rabani Bidgoli, M. (2020b), "Experimental study for ZnO nanofibers effect on the smart and mechanical properties of concrete", *Smart Struct. Syst.*, **25** (1), 97-104. https://doi.org/10.12989/sss.2020.25.1.097.
Kolahchi, R. and Kolahdouzan, F. (2021), "A numerical method for magneto-hygro-thermal dynamic stability analysis of defective quadrilateral graphene sheets using higher order nonlocal strain gradient theory with different movable boundary conditions", *Appl. Math. Model.*, **91**, 458-475. https://doi.org/10.1016/j.apm.2020.09.060.
Kolahchi, R., Keshtegar, B. and Trung, N.T. (2022), "Optimization of dynamic properties for laminated multiphase nanocomposite sandwich conical shell in thermal and magnetic conditions", *Int. J. Sandw. Struct.*, **24**, 643-662. https://doi.org/10.1177/10996362211020388.
Kolahdouzan, F., Mosayyebi, M., Ghasemi, F.A., Kolahchi, R. and Mousavi Panah, S.M. (2020), "Free vibration and buckling analysis of elastically restrained FG-CNTRC sandwich annular nanoplates", *Adv. Nano Res.*, **9**(4), 237-250. https://doi.org/10.12989/anr.2020.9.4.237.
Motezaker, M. and Kolahchi, R. (2017a), "Seismic response of SiO_2 nanoparticles-reinforced concrete pipes based on DQ and newmark methods", *Comput. Concr.*,**19**(6), 745-753. https://doi.org/10.12989/cac.2017.19.6.745.
Motezaker, M. and Kolahchi, R. (2017a), "Seismic response of concrete columns with nanofiber reinforced polymer layer", *Comput. Concr.*, **20**(3), 361-368. https://doi.org/10.12989/cac.2017.20.3.361.
Motezaker, M., Kolahchi, R., Kumar Rajak, D. and Mahmoud, S. R. (2021), "Influences of fiber reinforced polymer layer on the dynamic deflection of concrete pipes containing nanoparticle subjected to earthquake load", *Polym. Compos.*, **42**(8), 4073-4081. https://doi.org/10.1002/pc.26118.
Mosharrafian, F. and Kolahchi, R. (2016), "Nanotechnology, smartness and orthotropic nonhomogeneous elastic medium effects on buckling of piezoelectric pipes", *Struct. Eng. Mech.*, **58**(5), 931-947. https://doi.org/10.12989/sem.2016.58.5.931.
Naseri Taheri, M., Sabet, S.A. and Kolahchi, R. (2020), "Experimental investigation of self-healing concrete after crack using nano-capsules including polymeric shell and nanoparticles core", *Smart Struct. Syst.*, **25**(3), 337-343. https://doi.org/10.12989/sss.2020.25.3.337.
Taherifar, R., Zareei, S.A., Rabani Bidgoli, M. and Kolahchi, R. (2020), "Seismic analysis in pad concrete foundation reinforced by nanoparticles covered by smart layer utilizing plate higher order theory", *Steel Compos. Struct.*, **37**(1), 99-115. https://doi.org/10.12989/scs.2020.37.1.099.
Taherifar, R., Zareei, S.A., Rabani Bidgoli, M. and Kolahchi, R. (2021), "Application of differential quadrature and Newmark methods for dynamic response in pad concrete foundation covered by piezoelectric layer", *J. Comput. Appl. Math.*, **382**, 113075. https://doi.org/10.1016/j.cam.2020.113075.
Xu, H., Wang, Sh. and Hub, J. (2020), "Mass–spring–damper modeling and stability analysis of type-4 wind turbines connected into asymmetrical weak AC grid", *Energy Report*, **6**, 649-655. https://doi.org/10.1016/j.egyr.2020.11.161.
Zamanian, M., Kolahchi, R. and Rabani Bidgoli, M. (2017), "Agglomeration effects on the buckling behaviour of embedded concrete columns reinforced with SiO_2 nanoparticles", *Wind. Struct.*, **24**(1), 43-57. https://doi.org/10.12989/was.2017.24.1.043.
Zamani, A., Kolahchi, R. and Rabani Bidgoli, M. (2017), "Seismic response of smart nanocomposite cylindrical shell conveying fluid flow using HDQ-Newmark methods", *Comput. Concr.*, **20**(6), 671-682. https://doi.org/10.12989/cac.2017.20.6.671.
Zarei, M.S., Azizkhani, M.B., Hajmohammad, M.H. and Kolahchi, R. (2017), "Dynamic buckling of polymer–carbon nanotube–fiber multiphase nanocomposite viscoelastic laminated conical shells in hygrothermal environments", *J. Sandw. Struct. Mat.*, 1099636217743288. https://doi.org/10.1177/1099636217743288.
Žmindák, M., Pelagić, Z., Pastorek, P., Močilan, M. and Vybošťok, M. (2016), "Finite element modelling of high velocity impact on plate structures", *Procedia Eng.*, **136**, 162-168. https://doi.org/10.1016/j.proeng.2016.01.191.